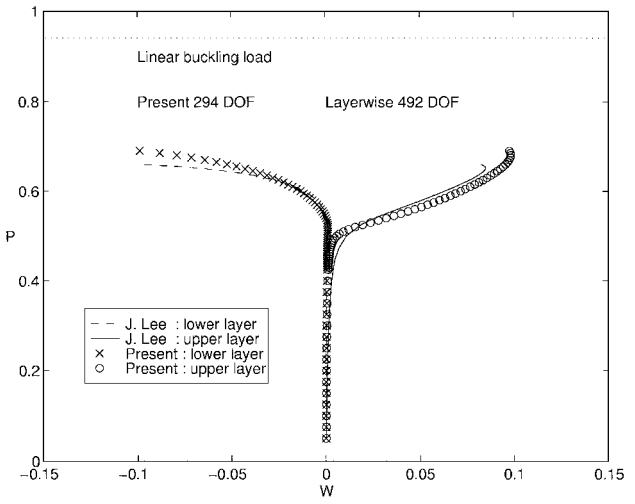

Fig. 5c Load-deflection curve of an $[0/90/90/0]_s$ laminate with simply supported ends.

unidirectional composite, the buckling load calculated from the linear bifurcation analysis is different from that of postbuckling analysis, as shown in Fig. 5b.

For a composite with simply supported ends, the load-deflection curves are shown in Fig. 5c. To satisfy the boundary condition, the initial imperfection is taken as $\xi = w_0 \sin(\pi x/L)$, $w_0 = 0.001$. Once more, the postbuckling response of this case is significantly different from that of the linear bifurcation analysis. In this case, the predicted linear buckling load significantly overestimates the global buckling of the structure.

However, the linear buckling loads may underestimate the global buckling load in the different stacking sequences, as reported in Ref. 5. From this observation, the linear bifurcation buckling loads are quite different from the results of the postbuckling analysis because they depend on the through-the-thickness position of delaminations, the stacking sequence, and the boundary conditions.

For the cross-ply cases, the results of the present global–local method show a slight deviation from those of the full layerwise model as the loads and deflections increase. However, the load-deflection curves of the present method agree reasonably well with those of the layerwise theory and the present model requires a smaller number of degrees of freedom than the layerwise model, as shown in Figs. 5b and 5c.

IV. Conclusions

In the present study, an efficient numerical model was developed to study the postbuckling behaviors of delaminated composites. The analysis was based on the one-dimensional beam-plate model with multiple delaminations.

A global–local approach for postbuckling problems with multiple delaminations was presented. A novel transition element between the layerwise element region and the first-order shear deformation zone was proposed by using a matching technique between first-order and layerwise models. This transition element is easy to implement and performs very well even in thick composites when proper shear correction factors in the first-order model are chosen.

The present numerical model and solution procedure consider the effect of initial imperfections and contact condition between delaminated surfaces. Although accurate postbuckling response can be performed by using layerwise-type theories, they require a great deal of computing time and memory. The proposed global–local method reduces the global degrees of freedom but still accurately models the delaminated zone. Thus it is suitable for the analysis of nonlinear behaviors of multiple delaminated composites.

It is expected that the realistic buckling and postbuckling behaviors of composite laminates with multiple delaminated imbedded cracks can be efficiently analyzed by the present global–local approach. This is now in progress.

Acknowledgment

This research was supported by the 1996 Inha University Research Fund. The authors gratefully acknowledge this support.

References

[1] Whitcomb, J. D., "Finite Element Analysis of Instability Related Delamination Growth," *Journal of Composite Materials*, Vol. 15, Sept. 1981, pp. 403–426.

[2] Reddy, J. N., "A Generalization of Two Dimensional Theories of Laminated Composite Plates," *Communications in Applied Numerical Methods*, Vol. 3, No. 3, 1987, pp. 173–180.

[3] Chai, H., Babcock, C. D., and Knauss, W. B., "One-Dimensional Modeling of Failure in Laminated Plates by Delamination Buckling," *International Journal of Solids and Structures*, Vol. 17, No. 11, 1981, pp. 1069–1083.

[4] Simitses, G. J., "Delamination Buckling of Flat Laminates," *Buckling and Postbuckling of Composite Plates*, edited by G. J. Turvey and I. H. Marshall, Chapman and Hall, London, 1995, pp. 299–328.

[5] Lee, J., Gürdal, Z., and Griffin, O. H., "Postbuckling of Laminated Composites with Delaminations," *AIAA Journal*, Vol. 33, No. 10, 1995, pp. 1963–1970.

[6] Barbero, E. J., "On a Generalized Laminate Plate Theory with Application to Bending, Vibration, and Delamination Buckling in Composite Laminates," Ph.D. Dissertation, Dept. of Engineering Science and Mechanics, Virginia Polytechnic Inst. and State Univ., Blacksburg, VA, Oct. 1989.

[7] Lee, J., "Vibration, Buckling and Postbuckling of Laminated Composites with Delaminations," Ph.D. Dissertation, Dept. of Engineering Science and Mechanics, Virginia Polytechnic Inst. and State Univ., Blacksburg, VA, May 1992.

[8] Cho, M., and Kim, J. S., "Bifurcation Buckling Analysis of Delaminated Composites Using Global-Local Approach," *AIAA Journal*, Vol. 35, No. 10, 1997, pp. 1673–1676.

[9] Chia, C. Y., *Nonlinear Analysis of Plates*, McGraw–Hill, New York, 1980, pp. 96–99.

[10] Kim, J. S., and Cho, M., "Matching Technique of Postprocess Method Using Displacement Fields of Higher Order Plate Theories," *Composite Structures*, Vol. 43, Dec. 1998, pp. 71–78.

G. A. Kardomateas
Associate Editor

Buckling of Filament-Wound Laminated Conical Shells Under Axial Compression

Liyong Tong*
University of Sydney,
Sydney, New South Wales 2006, Australia

Nomenclature

D_{ij} = terms in bending stiffness matrix
M_x = longitudinal bending moment
N_x = longitudinal membrane stress resultant
U = longitudinal displacement
V = circumferential displacement
W = transverse displacement
α = semivertex angle of the conical shell
θ = angle of fiber tow to the slant longitudinal direction in filament winding

I. Introduction

THE buckling behavior of isotropic and orthotropic conical shells under axially compressive loads and/or combined loads has been studied experimentally and analytically by many researchers.[1–7] However, for laminated composite conical shells there has been very limited literature available on experimental and analytical investigation of buckling behavior of composite laminated shells.[8–10] In this study, an experimental investigation is presented to discuss the buckling behavior of nine carbon-fiber-reinforced

Received Feb. 20, 1998; presented as Paper 98-1769 at the AIAA/ASME/ASCE/AHS/ASC 39th Structures, Structural Dynamics, and Materials Conference, Long Beach, CA, April 20–23, 1998; revision received Jan. 8, 1999; accepted for publication Feb. 5, 1999.

*Senior Lecturer, Department of Aeronautical Engineering. Member AIAA.

plastics (CFRP) and nine glass-fiber-reinforced plastics (GFRP) filament-wound conical shells subjected to axially applied compressive loads. The buckling loads and the related modes were first determined and then compared with the predicted results using an analytical solution procedure developed previously.

II. Specimen Preparation and Testing Procedure

There were nine CFRP and nine GFRP filament-wound truncated circular conical shell specimens, which were made using the horizontal helical filament winding machine and a stainless-steel conical shell mandrel that can be easily assembled or disassembled. The conical shell mandrel had a semivertex angle α of 9 deg, and its outer surface had a diameter of 265 mm at its small end, a diameter of 328 mm at its large end, and a slant length of 200 mm. Note that dimensions of the inner wall of the specimens are identical to those of the outer surface of the mandrel, whereas the diameter of the shell specimens on the neutral plane should be equal to the inner diameter plus the wall thickness.

In the filament-winding process, a single fiber tow runs repetitively from one pole to the other to form one over-and-underwoven fabric layer, which can be approximated as two single plies with fibers equally distributed in the both directions, i.e., $\pm\theta$. When the fiber orientation is not 0 or 90 deg, it varies as the fiber tow runs along the longitudinal direction. Thus for simplicity, a nominal fiber orientation for a ply is defined as the fiber orientation at the midlength of the conical shell mandrel. The nominal layups or fiber orientations for both CFRP and GFRP specimens are given in Table 1. The average fiber volume fractions for specimens C-1-*i*, C-2-*i*, C-3-*i*, G-1-*i*, G-2-*i*, and G-3-*i* ($i = 1, 2, 3$) are 47.7, 45.8, 48.7, 50.6, 49.5, and 51.0%, respectively. The average mechanical properties of a single ply of the same fiber volume fractions for both types of specimens are listed in Table 2.

Inspection of the 18 shell specimens revealed that they have the following structural characteristics: 1) The wall thickness of each shell specimen is constant in the circumferential direction, and it varies only in the longitudinal direction, i.e., is thicker at the small end and thinner at the large end; and 2) the fiber orientation in each fabric layer remains the same in the circumferential direction; however, it decreases along the longitudinal direction, i.e., the fiber angle is larger at the small end and is smaller at the large end. In addition, two rings made of 90-deg fiber tows were attached to both ends of each conical shell specimen to reinforce locally the shell specimens and to prevent a premature local end brooming type of failure prior to global buckling of the shells. The thickness for all specimens was measured at both ends of the shells at every 30 deg along the circumferential direction, and an average value was then taken as the nominal thickness. Tables 3 and 4 list the thickness t of the specimens at both small and large ends for CFRP and GFRP specimens, respectively.

Table 1 Nominal layups for all specimens

Group number	Specimen ($i = 1, 2, 3$)	Layup
1	C-1-*i*; G-1-*I*	(±30/±45/±30 deg)
2	C-2-*i*; G-2-*I*	(90/±45/90 deg)
3	C-3-*i*; G-3-*I*	(90/±30/90 deg)

Table 2 Nominal mechanical properties of a ply

Material	GFRP	CFRP
Longitudinal modulus, GPa	42.6	97.5
Transverse modulus, GPa	11.7	8.3
Shear modulus, GPa	4.8	4.1
Poisson ratio	0.302	0.32

The test apparatus used comprised two parts: One was the loading system that was used to apply and control the axial compressive load and to realize simply supported boundary conditions at both ends of the shells; and the other was the measuring system, which was used to record the strains and displacements at different load levels as well as the axial compressive load and the axial end shortening. The loading system consisted of an MTS-880 material testing system and a pair of thick, flat loading disks, as described in detail in Tong.[10]

Four strain gauge rosettes and four displacement transducers were placed every 90 deg along the circumference of the middle height section of the shells. The four strain gauge rosettes were used to monitor uniformity of the axially applied compressive load. A multichannel data acquisition system was used to record the strain gauges and the displacement transducers. In addition, the curves of the axially compressed load vs the axial end shortening were also recorded.

The test procedure included the following steps: 1) Install the loading disks properly to ensure that they are perpendicular to the loading axis and are parallel to each other; 2) mount specimen to ensure that proper V channels be formed to realize approximately the simply supported boundary conditions at both ends; and 3) connect the displacement transducers and strain gauges to the multichannel data logger, calibrate the system, and then start loading via displacement control at a loading rate of about 0.5 mm/min. For each specimen the following two stages were employed:

Stage 1. Determination of buckling load and mode: The curve of the axial load vs the axial displacement for each specimen was recorded using the X-Y recorder available in the MTS-880 testing system. Readings of the strain gauges and the displacement transducers were obtained via the data logger at different load levels to monitor the strain distribution and to detect buckling of the specimen. The initial buckling load and mode of each specimen were obtained in this stage. After initial buckling, the specimen was then fully unloaded to its initial state.

Stage 2. Effect of damage caused by initial buckling: The initially buckled specimen was then loaded again to determine the residual buckling load and mode of the damaged specimen. The maximum value of the applied axial displacement was, however, limited to the maximum displacement applied to a specimen when it first buckled and then unloaded. This procedure was repeated for some specimens to study the effect of the damage that incurred when the specimen first buckled on the residual buckling load of the specimen.

III. Results and Discussion

For all specimens in all load cycles, the applied load increased linearly with the axial end shortening or crosshead movement until the specimen buckled in the typical diamond buckling shape. Figure 1 shows photographs of typical buckling modes for the specimens in

Table 3 Buckling load P_{CR} (kN) of CFRP conical shells

Specimen	Thickness at small end, mm	Thickness at large end, mm	Measured buckling load	Predicted buckling load, S3	Predicted buckling load, C3
C-1-1	2.43	2.19	232.5 (5,1)	227.8	457.7
C-1-2	2.30	1.90	196.2 (6,1)	186.7	376.1
C-1-3	1.80	1.60	141.5 (7,1)	117.3	245.6
C-2-1	1.19	1.15	28.6 (8,2)	27.9	52.9
C-2-2	1.21	1.09	27.0 (8,2)	29.2	56.6
C-2-3	1.15	1.09	35.3 (9,2)	25.5	51.6
C-3-1	1.24	1.08	49.6 (7,2)	46.8	82.0
C-3-2	1.28	1.12	56.0 (9,2)	50.2	86.7
C-3-3	1.21	1.12	52.7 (10,2)	45.7	80.2

Table 4 Buckling load P_{CR} (kN) of GFRP conical shells

Specimen	Thickness at small end, mm	Thickness at large end, mm	Measured buckling load	Predicted buckling load, S3	Predicted buckling load, C3
G-1-1	1.91	1.65	145.0 (6,1)	84.8	174.0
G-1-2	1.91	1.61	138.1 (6,1)	77.4	159.3
G-1-3	1.81	1.50	103.2 (6,1)	69.0	139.7
G-2-1	1.16	1.01	21.3 (7,2)	20.1	35.3
G-2-2	1.12	1.04	23.5 (9,2)	20.2	35.8
G-2-3	1.18	1.10	29.6 (8,2)	25.3	41.2
G-3-1	1.28	1.08	43.5 (8,2)	39.2	62.1
G-3-2	1.43	1.17	49.5 (7,2)	45.1	85.2
G-3-3	1.09	1.05	33.7 (8,2)	31.4	56.7

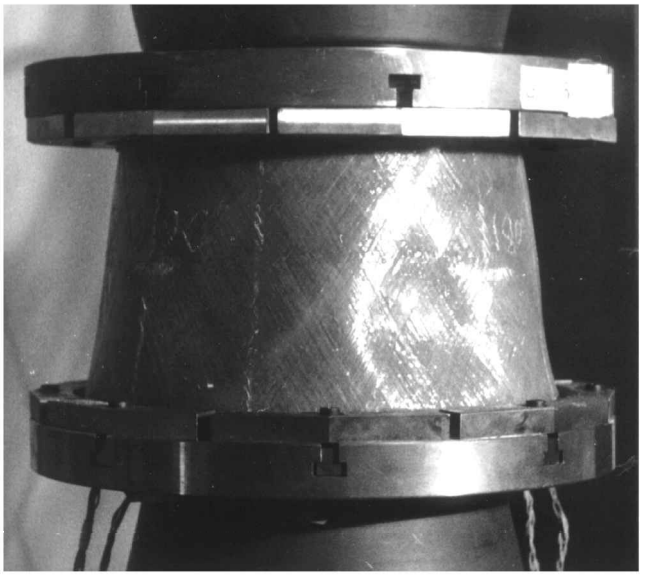

a) Specimen group 1

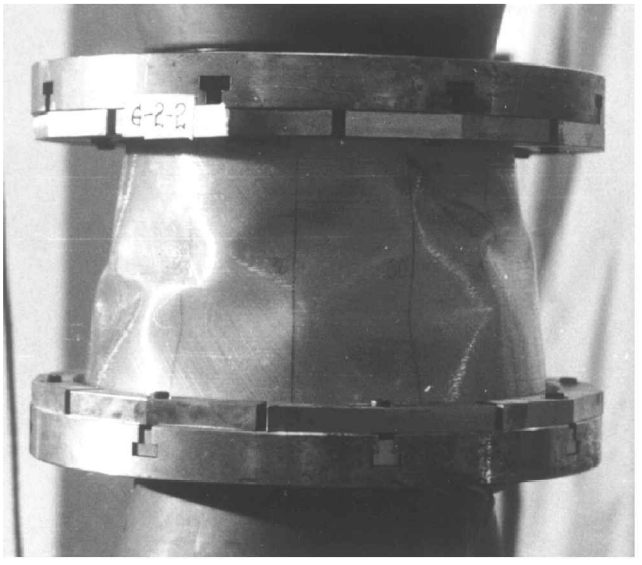

b) Specimen groups 2 and 3

Fig. 1 Typical buckling modes.

specimen group 1 and specimen groups 2 and 3, respectively. In the longitudinal direction there was only one half sine wave for specimens in group 1, and there were two half sine waves for those in specimen groups 2 and 3. This is because specimens in group 1 are generally thicker than specimens in groups 2 and 3.

The typical readings of the strain gauges in the longitudinal (ε_0 deg) and circumferential (ε_{90} deg) directions for all specimens at various load levels during the first load cycle reveal that the longitudinal strain ε_0 deg distributes in a relatively uniform pattern in the circumferential direction, which indicates that the applied axial load was uniform.

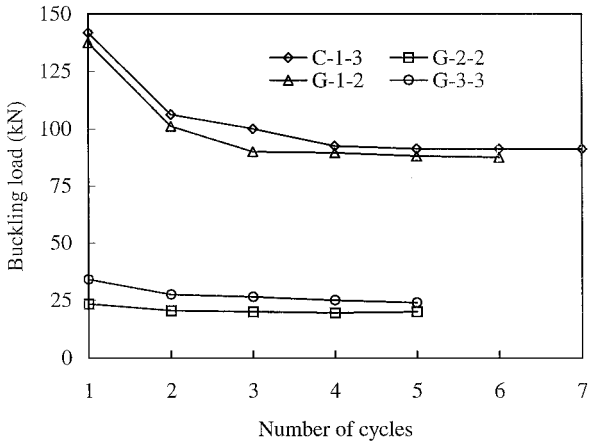

Fig. 2 Buckling loads vs the number of loading cycles for specimens C-1-3, G-2-2, G-1-2, and G-3-3 with maximum applied displacements of 1.5, 1.5, 2, and 1.1 mm, respectively.

The buckling loads and modes of the first load cycle are given in Tables 3 and 4 for all CFRP and GFRP specimens, respectively. The numbers in the parentheses represent the half wave numbers in the circumferential and longitudinal directions, respectively, e.g., for specimen C-1-1 there were five half waves in the circumferential direction and only one half wave in the longitudinal direction. Evidently, buckling loads of CFRP specimens are generally larger than those of GFRP specimens when both have the same ply-stacking sequence. This can readily be explained by saying that the CFRP is generally regarded to be stiffer and stronger than the GFRP. The specimens with (±30/±45/±30 deg) layup buckle at larger loads than specimens with (90/±30/90 deg) layup, which have higher buckling loads than a specimen with (90/±45/90 deg) layup. This is because the specimen possesses higher load-carrying capacity when more fibers are placed in or close to the load path direction. Results in the third column reveal that specimen group 1 (±30/±45/±30 deg) has the largest buckling-load-to-weight ratio and thus has the highest stiffness-to-weight ratio; specimen group 2 has the smallest buckling-load-to-weight ratio. Also note that specimens in group 1 buckled into only one half wave in the longitudinal direction, whereas specimens in groups 2 and 3 buckled into two half waves. In addition, the circumferential half wave numbers for specimens in group 1 are lower than those in groups 2 and 3.

In the subsequent loading cycles after the initial buckling, the maximum applied cross-head movement was kept to the level attained in the first loading cycle. In doing so, the effect of the damage incurred in the first buckling procedure on the residual buckling load was investigated. Figure 2 plots the buckling load vs the number of cycles for specimens C-1-3, G-2-2, G-1-2, and G-3-3, with maximum applied displacements of 1.5, 1.5, 2, and 1.1 mm, respectively. The buckling loads for these buckling cycles are considerably lower than the initial buckling load because of the existence of the buckling damage incurred in the initial buckling. However, by limiting

the maximum applied axial displacement to the value applied in the initial buckling, the residual buckling load tends to approach a plateau.

IV. Comparison Between Analysis and Experimental Results

To model the testing situation, we calculate the buckling load using the following simply supported boundary conditions (S3) at the small and large ends, respectively:

$$N_x = V = M_x = W = 0 \tag{1a}$$

$$N_x = V = M_x = U\sin\alpha - W\cos\alpha = 0 \tag{1b}$$

For comparison we also calculate the buckling load using the following clamped boundary conditions (C3) at the small and large ends, respectively:

$$N_x = V = \frac{\partial W}{\partial x} = W = 0 \tag{2a}$$

$$N_x = V = \frac{\partial W}{\partial x} = U\sin\alpha - W\cos\alpha = 0 \tag{2b}$$

Buckling loads and the corresponding buckling modes were calculated for both simply supported (S3) and clamped (C3) conditions using the solution procedure developed by Tong and Wang[8] and the material properties in Table 2. In all calculations, an average thickness is used for each specimen,[10] and the coupling terms D_{16} and D_{26} are neglected as they are relatively small compared to bending terms D_{11}, D_{12}, D_{22}, and D_{66}.

Tables 3 and 4 tabulate the measured buckling loads and modes as well as those predicted using the analytical solution procedure and the two types of boundary conditions for all specimens. Evidently, the buckling loads of all CFRP and most GFRP (except for G-1-i, $i = 1, 2, 3$) specimens predicted using the simply supported boundary condition S3 have a better agreement to those measured compared with those predicted using the clamped boundary condition C3. The buckling loads predicted using the S3 conditions are generally lower than those measured, whereas those predicted using the C3 conditions are much higher than the measured ones. This result indicates that the real boundary condition should be somewhere between both S3 and C3 boundary conditions. The analysis using the S3 boundary conditions predicted that all shells buckle at an axisymmetrical mode that is quite different from the experimental observation. Another important factor responsible for the existing discrepancies could be the geometrical imperfections that were not measured in this program because of limited facilities and were not included in the analysis.

V. Conclusions

An experimental and analytical investigation is presented to study buckling behavior of axially compressed conical shells. The present results show that 1) specimens with a layup of (±30/±45/±30 deg) buckle at higher buckling loads than those with (90/±30/90 deg), which subsequently have higher buckling loads than specimens with a layup of (90/±45/90 deg); 2) damage caused during initial buckling of the shells can significantly decrease the buckling load of the subsequent buckling; and 3) analytical solutions using the nominal ply angle and thickness of the shell at the midlength can be used with the S3 boundary condition to predict the buckling loads, which were found to correlate reasonably well with the measured ones.

References

[1] Seide, P., "Axisymmetrical Buckling of Circular Cones Under Axial Compression," *Journal of Applied Mechanics*, Vol. 23, No. 4, 1956, pp. 625–628.

[2] Lackman, L., and Renzien, J., "Buckling of Circular Cones Under Axial Compression," *Journal of Applied Mechanics*, Vol. 27, No. 3, 1960, pp. 458–460.

[3] Singer, J., "Buckling of Circular Conical Shells Under Uniform Axial Compression," *AIAA Journal*, Vol. 3, No. 5, 1965, pp. 985–987.

[4] Baruch, M., Harari, O., and Singer, J., "Low Buckling Loads of Axially Compressed Conical Shells," *Journal of Applied Mechanics*, Vol. 37, No. 2, 1970, pp. 384–392.

[5] Tani, J., and Yamaki, Y., "Buckling of Truncated Conical Shells Under Axial Compression," *AIAA Journal*, Vol. 8, No. 3, 1970, pp. 568–570.

[6] Weingarten, V. I., Morgan, E. J., and Seide, P., "Elastic Stability of Thin Walled Cylindrical and Conical Shells Under Axial Compression," *AIAA Journal*, Vol. 3, No. 3, 1965, pp. 500–505.

[7] Kojima, K., Ichida, K., and Sunakawa, M., "An Experimental Investigation on the Buckling of Truncated Conical Shells Under Axial Compression," *Journal of Japan Society of Aeronautics and Aerospace*, Vol. 21, No. 228, 1973, pp. 32–38.

[8] Tong, L., and Wang, T. K., "Simple Solutions for Buckling of Laminated Conical Shells," *International Journal of Mechanical Sciences*, Vol. 34, No. 2, 1992, pp. 93–111.

[9] Giavotto, V., Poggi, C., Chryssanthopoulos, M., and Dowling, P., "Buckling Behaviour of Composite Shells Under Combined Loading," *Buckling of Shell Structures, On Land, In the Sea and In the Air*, edited by J. F. Jullien, Elsevier Applied Science, Oxford, England, UK, 1991, pp. 53–60.

[10] Tong, L., "Buckling of Filament Wound Composite Conical Shells Under Axial Compression," AIAA Paper 98-1769, April 1998.

G. A. Kardomateas
Associate Editor